Development of New Oxygen Ion Conductors Based on Nd_4GeO_8 and Nd_3GaO_6

Ram Dayal Purohit,† Anthony Chesnaud, Abdessadek Lachgar,‡ Olivier Joubert, Maria Teresa Caldes, Yves Piffard,* and Luc Brohan

Institut des Matériaux Jean ROUXEL, UMR CNRS, Université de Nantes no. 6502 2, rue de la Houssinière, BP 32229-44322 Nantes Cedex 3, France

Received March 9, 2005. Revised Manuscript Received June 6, 2005

New oxygen ion conductors have been prepared by substituting Ga^{3+} for Ge^{4+} in Nd_4GeO_8, Zn^{2+} and Mg^{2+} for Ga^{3+} in Nd_3GaO_6, and Ca^{2+} and Sr^{2+} for Nd^{3+} in Nd_3GaO_6. A combustion technique using ethylenediamine tetraacetic acid has been developed to synthesize these materials at ∼900 °C, leading to powders with spherical particles of about 100−200 nm. The green pellets obtained through the combustion-synthesized powders could be sintered to ∼98% at 1250 °C. It was found that $Nd_4Ge_{1-x}Ga_xO_{8-x/2}$ are formed up to $x = 0.10$, $Nd_3Ga_{1-x}M_xO_{6-x/2}$ (M = Zn, Mg) up to $x = 0.03$, and $Nd_{3(1-x)}M'_{3x}GaO_{6-3x/2}$ up to $x = 0.03$ and 0.015 for M′ = Ca and Sr, respectively. These relatively small substitution rates induce a significant increase in oxygen ion conductivity ($\sigma_{800°C} = 0.2 \times 10^{-2}$ S cm^{-1} for $Nd_4Ge_{0.9}Ga_{0.1}O_{7.95}$; $\sigma_{800°C} = 0.5 \times 10^{-2}$ and 0.4×10^{-2} S cm^{-1} for $Nd_3Ga_{0.97}M_{0.03}O_{5.985}$ with M = Zn and Mg, respectively, and $\sigma_{800°C} = 0.6 \times 10^{-2}$ and 0.7×10^{-2} S cm^{-1} for $Nd_{2.91}Ca_{0.09}GaO_{5.955}$ and $Nd_{2.955}Sr_{0.045}GaO_{5.9775}$, respectively) with respect to pure Nd_4GeO_8 ($\sigma_{800°C} = 2.8 \times 10^{-4}$ S cm^{-1}) and pure Nd_3GaO_6 ($\sigma_{800°C} = 2.7 \times 10^{-4}$ S cm^{-1}).

1. Introduction

In the present solid oxide fuel cells (SOFCs) the favored electrolyte is yttria-stabilized zirconia (YSZ), which exhibits high oxygen ion conductivity at rather high temperature (≥800 °C). As a consequence, the operating temperature of YSZ-based SOFCs must be high (850−1000 °C), and although there are advantages to operating at high temperature, this does induce severe restrictions upon the materials that can be used reliably due to problems associated with thermal cycling and performance degradation that results from increased reactivity of the individual components at higher temperatures. Therefore, there is a great deal of interest in the development of new materials with improved properties that could enable lower-temperature operation.

Since the discovery of fast oxygen ion conduction in YSZ, fluorite-like compounds have been extensively investigated and metal substitution with lower valent cations to form or increase charge-compensating oxygen vacancies has become one of the most common approaches to enhancing oxygen ion conductivity. As part of these continuing efforts to find new electrolyte materials, the principle mentioned above has been applied to Nd_4GeO_8[1] and Nd_3GaO_6.[2,3]

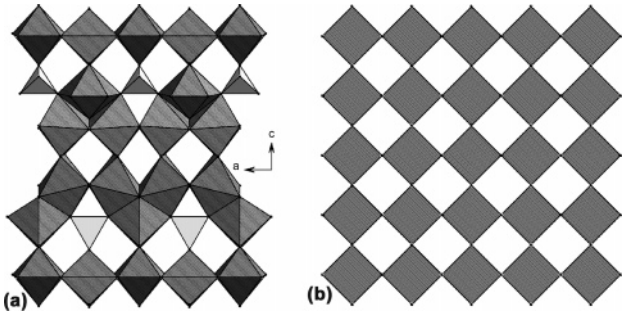

Figure 1. [010] view of (a) a fragment of the $Nd_4O_4GeO_4$ structure and (b) the cubic fluorite structure.

Nd_4GeO_8 is a neodymium oxy-monogermanate that is better formulated as $Nd_4O_4GeO_4$. Its structure [space group (SG) $Pmc2_1$ with $a = 7.475(2)$ Å, $b = 5.727(2)$ Å, and $c = 17.927(5)$ Å] is built up from six kinds of edge-sharing NdO_7 polyhedra forming a three-dimensional framework to which GeO_4 tetrahedra are bonded via vertexes (Figure 1a). Inclusion of one next-neighbor oxygen atom in the coordination sphere of each Nd atom enables the structure of $Nd_4O_4GeO_4$ to be considered as consisting of NdO_8 distorted cubes and a fluorite-like packing of O atoms to be recognized (Figure 1b).[1] This structural feature prompted us to investigate the possibility of creating oxide ion vacancies by substitution of Ga^{3+} for Ge^{4+}, to evaluate the potential of the oxygen-deficient compounds as solid electrolytes. Attempts to substitute alkali-earth cations for Nd^{3+} resulted in new phases which are presently being identified.

Nd_3GaO_6 is a neodymium oxy-monogallate whose chemical formula can be better written as $Nd_3O_2GaO_4$. Its structure[3] (SG $Cmc2_1$ with $a = 9.1820(1)$ Å, $b = 11.5396(1)$ Å, $c = 5.5748(1)$ Å) is built up from two kinds of edge-sharing

* To whom correspondence should be addressed. E-mail: piffard@cnrs-imn.fr.
† Present address: Powder Metallurgy Division, Bhabha Atomic Research Center, Vashi Complex, Navi Mumbai 400 705, India.
‡ Present address: Department of Chemistry, Wake Forest University, Winston-Salem, NC 27109.

(1) Merinov, B. V.; Masimov, B. A.; Dem'yanets, D. N.; Belov, N. V. *Sov. Phys. Dokl.* **1978**, *23* (7), 452.
(2) Coutures, J.; Nicolas, J.; Antic, E.; Schiffmacher, G.; Coutures, J.-P. *C. R. Acad. Sci. Paris Ser. II* **1983**, *296*, 347.
(3) Liu, F. S.; Liu, Q. L.; Liang, J. K.; Yang, L. T.; Song, G. B.; Luo J.; Rao, G. H. *J. Solid State Chem.* **2004**, *177*, 1796.

10.1021/cm050537h CCC: $30.25
Published on Web 07/27/2005

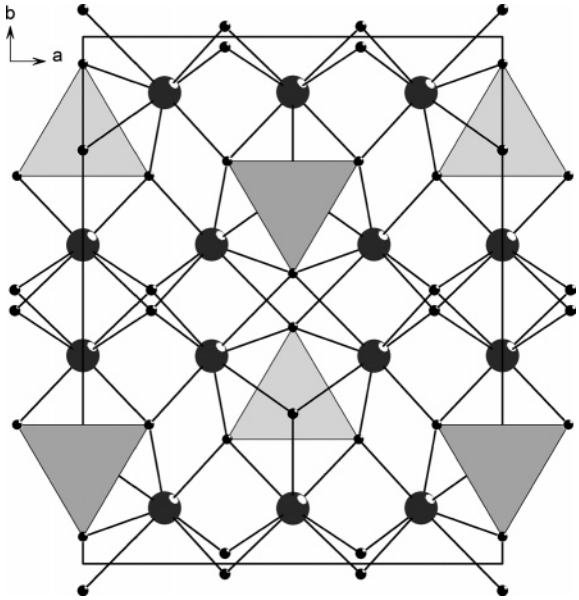

Figure 2. [001] view of the $Nd_3O_2GaO_4$ structure showing GaO_4 tetrahedra, Nd (large black circles), and O atoms (small black circles).

NdO_7 polyhedra forming a three-dimensional framework to which GaO_4 tetrahedra are bonded via vertexes (Figure 2). As in the case of $Nd_4O_4GeO_4$, formation of vacancies on oxygen sites coordinated to Nd^{3+} cations only can be expected as a result of the large coordination number of neodymium. Therefore, attempts to create oxygen vacancies were made and the potential of the oxygen-deficient phases as solid electrolytes was evaluated.

In solid-state synthesis of compounds with small substitution rates, the major problems are local stoichiometric variations and the requirement of a high calcination temperature which leads to bigger particle size and poor sinterability of the powders. These problems can be overcome to some extent by applying tedious and time-consuming repeated grinding and calcinations steps. A variety of wet-chemical processes have been developed to deal with the shortcomings of solid-state synthesis. However, most of them suffer from disadvantages such as use of expensive and moisture-sensitive metal alkoxides in the case of sol−gel, repeated washing in the case of coprecipitation, and so forth. In addition, in most cases, the end product consists of hard agglomerates which require a post-milling step.

In recent years, the combustion technique has attracted a considerable attention because of its capability to deliver phase-pure, ultrafine powders at low calcination temperature which can be readily sintered to high density at a comparatively lower temperature.[4,5] The technique involves an exothermic decomposition of a homogeneous fuel−oxidant precursor (mostly in the form of a gel) that results in either finely divided powder of the required phase or semi-decomposed precursors containing considerable carbonaceous residue, depending on the nature and amount of fuel used in the process.[6,7] The success of the process is attributed to an atomistic level blending among the constituents, achieved by using a suitable complexing agent [e.g., citric acid, ethylenediamine tetraacetic acid (EDTA), urea, glycine, etc.] and an exothermic redox reaction between the fuel and an oxidizer (i.e., nitrates). Urea, glycine, and citric acid are the common fuels used in the combustion technique, whereas a few papers report the use of EDTA as a fuel in the combustion technique. However, the versatile ability of EDTA as a complexing agent for a variety of metal ions is well-known. It enables a transparent viscous gel to be obtained by preventing selective precipitation. Furthermore, it can combust with nitrates at low ignition temperature also and, hence, is a good choice as a fuel for the combustion process.

The present paper reports the development of new oxygen ion conductors based on substitutions of Ga^{3+} for Ge^{4+} in $Nd_4O_4GeO_4$, Zn^{2+} and Mg^{2+} for Ga^{3+} in $Nd_3O_2GaO_4$, and Ca^{2+} and Sr^{2+} for Nd^{3+} in $Nd_3O_2GaO_4$, using the newly developed EDTA−nitrate combustion process and their characterization in terms of phase purity, grain size, sinterability, and anionic conductivity.

2. Experimental Section

All materials used were of analytical reagent grade. Initially, attempts have been made to synthesize $Nd_4O_4GeO_4$-based and $Nd_3O_2GaO_4$-based materials through the conventional solid-state reaction (the terms "$Nd_4O_4GeO_4$- and $Nd_3O_2GaO_4$-based materials" are used throughout the manuscript for both pure and substituted $Nd_4O_4GeO_4$ and $Nd_3O_2GaO_4$ phases). The weighed quantities of corresponding oxides were mixed in an agate mortar, ground in acetone, and calcined at 1200 °C for 24 h. The calcined powders of $Nd_4O_4GeO_4$- and $Nd_3O_2GaO_4$-based materials were ground, made into pellets, and fired at 1400 and 1250 °C, respectively, for 72 h.

For the synthesis of $Nd_4O_4GeO_4$ and $Nd_3O_2GaO_4$ through the EDTA−nitrate combustion technique, separate aqueous solutions of metal nitrates and EDTA were prepared. Neodymium nitrate solution was prepared by dissolving Nd_2O_3 in a minimum volume of dilute HNO_3. Because GeO_2 is not soluble in an acidic medium, it was first dissolved in a minimum volume of dilute aqueous ammonia. The complex formed is soluble in a nitric medium. The aqueous solution of gallium nitrate was prepared from $Ga(NO_3)_3 \cdot xH_2O$. Prior to its use, the exact composition of this latter material was analyzed by performing thermogravimetric analysis (TGA). The EDTA ($C_{10}H_{16}N_2O_8$) solution was prepared by dissolving its required quantity in a minimum volume of dilute aqueous ammonia. The solutions of metal nitrates and EDTA were mixed together in the required molar ratio to obtain transparent metal nitrate−EDTA solutions. The molar ratio of total metal ions to EDTA was maintained at 1:0.5.

As an example, the metal nitrate−EDTA solution that was used for the synthesis of 2×10^{-3} mol (1.553 g) of $Nd_4Ge_{0.9}Ga_{0.1}O_{7.95}$ was prepared as follows: 1.3459 g (4×10^{-3} mol) of Nd_2O_3 was dissolved at ∼80 °C in 40 mL of a 0.785 M solution of HNO_3 (i.e., with an excess of ∼30% in HNO_3 with respect to the formation of Nd^{3+} nitrate, to ensure complete and rather fast dissolution of the oxide) and 20 mL of a 10^{-2} M aqueous solution of $Ga(NO_3)_3 \cdot xH_2O$ was added to this Nd^{3+} solution. Then, 0.1883 g (1.8×10^{-3} mol) of GeO_2 was dissolved at ∼80 °C in 24 mL of an aqueous 1 M solution of ammonia, and this solution was poured slowly into

(4) Schafer, J.; Sigmund, W.; Roy, S.; Aldinger, F. *J. Mater. Res.* **1997**, *12*, 2518.
(5) Bhaduri, S.; Bhaduri, S. B.; Zhou, E. *J. Mater. Res.* **1998**, *13*, 156.
(6) Purohit, R. D.; Sharma, B. P.; Pillai, K. T.; Tyagi, A. K. *Mater. Res. Bull.* **2001**, *36*, 2711.
(7) Purohit, R. D.; Tyagi, A. K. *J. Mater. Chem.* **2002**, *2*, 312.

the beaker containing the Nd^{3+}/Ga^{3+} solution under continuous stirring. The EDTA solution was prepared by dissolving 1.4612 g (5×10^{-3} mol) of the solid in 10 mL of an aqueous 1 M solution of ammonia. It was added to the metal nitrate solution under stirring.

The thermal dehydration of metal nitrate−EDTA solutions (at ~100 °C on a hot plate) resulted in a highly viscous gel. As soon as the gel is formed, the temperature of the hot plate was increased to ~300 °C. At this stage, the gel swelled and auto-ignited in a controlled and self-sustaining manner with the evolution of a large volume of gases to produce voluminous blackish powder hereafter termed as the precursor. The Zn^{2+} and Mg^{2+} substituted compounds were prepared in a similar way using $Zn(CH_3COO)_2 \cdot xH_2O$ and $Mg(NO_3)_3 \cdot xH_2O$ as their corresponding raw materials. The exact amount of water in these materials was determined by TGA before their use. Calcium and strontium nitrate solutions were prepared by decomposition of the corresponding carbonates in a minimum volume of dilute HNO_3.

The precursors obtained after auto-ignition were calcined at various temperatures to remove the carbonaceous residues and to determine phase evolution. X-ray diffraction (XRD) patterns of the combustion-synthesized powders were recorded on a Siemens D5000 diffractometer using Cu Kα radiation.

The combustion synthesized powders of $Nd_4O_4GeO_4$- and $Nd_3O_2GaO_4$-based materials were ground in acetone for 5 min using a pestle and mortar and then cold-pressed in the form of 10-mm-diameter pellets at a pressure of 1 kbar using a uniaxial hydraulic press. Stearic acid was used as a lubricant. Sintering was performed in air at 1250 °C for 4 h at a 10 °C/min heating rate.

The XRD patterns of the sintered samples were recorded at room temperature using an INEL position-sensitive detector (Cu Kα1: $\lambda = 1.540\,598$ Å). Refinements of cell parameters were carried out using the program FULLPROF[8] in the full pattern matching mode, and its interface is the program WinPLOTR.[9]

Densities of sintered materials were determined by measuring the dimensions and weight of the pellets. The morphology and microstructure studies on combustion-synthesized powders and sintered pellets were carried out using a JEOL JSM 6400F scanning electron microscope. Energy-dispersive X-ray (EDX) analyses were systematically performed on numerous single crystals with a Link System OXFORD analyzer.

Conductivity measurements were made with the use of samples in the form of pellets using a model 1260 high-frequency response analyzer of M/s Solartron (Schlumberger, U.K.) with a 500 mV of alternating current (ac) perturbation, from 0.01 Hz to 2 MHz, between 250 and 800 °C, in dry air. Both sides of the pellets were coated with Pt paste acting as electrodes. Some measurements were also made under reduced oxygen partial pressures [10^{-5} atm using N_2 from the laboratory network, and 10^{-20} atm with an $Ar-H_2$ (5%) gaz mixture] which were measured with the use of a YSZ-based oxygen sensor placed next to the pellet. The complex impedance spectra were analyzed with Zview (Scribner Associates, Inc.) and MicW[10] electrochemical impedance softwares.

3. Results and Discussion

3.1. Investigation of Synthesis and Sintering Conditions. When $Nd_4O_4GeO_4$ materials were prepared by solid-state reaction and sintered at 1400 °C, the pellet densities were found to be 80%, which is too low for accurate measurements of the ionic conductivity.

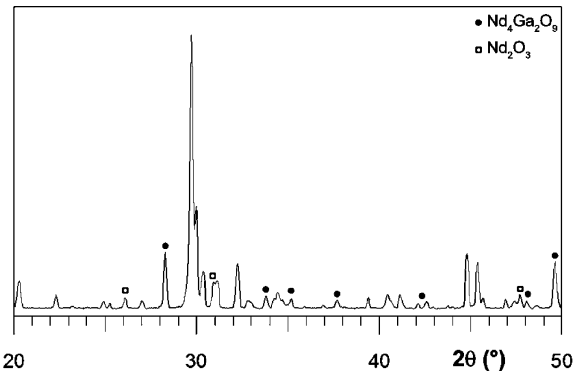

Figure 3. Synthesis of $Nd_3O_2GaO_4$ by solid-state reaction: XRD pattern of a sample heated at 1250 °C for 72 h, showing $Nd_4Ga_2O_9$ and Nd_2O_3 as impurity phases along with $Nd_3O_2GaO_4$ as a major phase.

Initial attempts to synthesize $Nd_3O_2GaO_4$-based materials through conventional solid-state reaction were not successful as result of the easy formation of the stable intermediate cuspidine type compound $Nd_4Ga_2O_9$.[11] Figure 3 shows the XRD pattern of the sample calcined at 1250 °C for 72 h, which reveals $Nd_4Ga_2O_9$ and Nd_2O_3 as impurity phases along with $Nd_3O_2GaO_4$ as a major phase. Rao et al.[3] also faced the same problem during the synthesis of $Nd_3O_2GaO_4$ through solid-state reaction.

Because phase purity, homogeneous distribution of substituents, and well-sintered samples affect the conducting characteristics significantly, attempts have been made to synthesize $Nd_4O_4GeO_4$- and $Nd_3O_2GaO_4$-based materials through the newly developed EDTA−nitrate combustion technique. Generally, the amount of fuel used in the combustion process is decided by using the principle of propellant chemistry,[12] according to which, for a stoichiometric combustion reaction, the coefficient of total oxidizing valency of metal nitrate to total reducing valency of fuel should be unity.

To prepare powder in a somewhat larger quantity without leaving any flame/fire and powder outside the beaker, controlling the combustion reaction is an equally important aspect of the process. Fuel-deficient and stoichiometric combustion reactions are normally highly exothermic and, hence, difficult to control.[4,13] To control the combustion kinetics, a fuel-rich composition was used.[3,4] Hence, a large excess of EDTA was used to control the combustion reactions for the synthesis of $Nd_4O_4GeO_4$- and $Nd_3O_2GaO_4$-based materials. The combustion reactions were found to occur in a self-sustaining and controlled manner when a total metal ions to EDTA molar ratio of 1:0.5 was used. However, the products contained considerable amount of carbonaceous residues and were amorphous in nature as indicated by the XRD pattern of the as-prepared powder obtained during the

(8) Roisnel, T.; Rodríguez-Carvajal, J. FULLPROF. *Physica B* **1993**, *192*, 55 (see also http://www-llb.cea.fr/fullweb/fp2k/fp2k.htm).
(9) Roisnel, T.; Rodríguez-Carvajal, J. WinPLOTR: a Windows tool for powder diffraction patterns analysis. In *Materials Science Forum*, Proceedings of the 7th European Powder Diffraction Conference (EPDIC 7); Delhez, R., Mittenmeijer, E. J., Eds.; 2000, pp 118−123 (see also http://www-llb.cea.fr/fullweb/winplotr/winplotr.htm).
(10) Suchaud, M. *MicW (v. 2.0): A Windows tool for measurement and analysis of complex impedance data*; Nantes, 2004 (contact: michel.suchaud@cnrs-imn.fr).
(11) Schneider, S. J.; Roth, R. S.; Waring, J. L. *J. Res. Natl. Bur. Stand. (U.S.)* **1961**, *65A*, 345.
(12) Jain, S. R.; Adiga, K. C.; Pai Verneker, V. R. *Combust. Flame* **1981**, *40*, 71.
(13) Sousa, V. C.; Segadaes, A. M.; Morelli, M. R.; Kiminami, R. H. G. A. *Int. J. Inorg. Mater.* **1999**, *1*, 235.

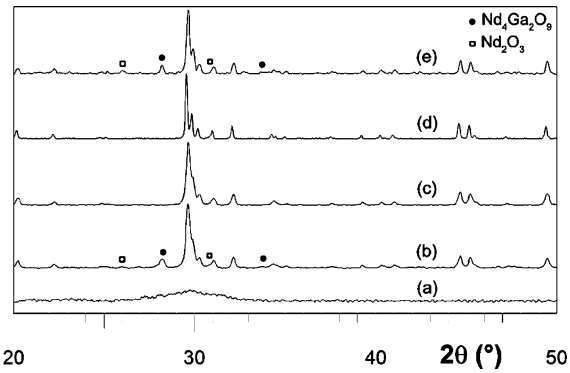

Figure 4. XRD pattern of (a) as-prepared powder obtained during the combustion synthesis of $Nd_3O_2GaO_4$, (b) as-prepared powder plus calcination at 800 °C for 4 h (showing trace amounts of $Nd_4Ga_2O_9$ and Nd_2O_3), (c) as-prepared powder plus calcination at 900 °C for 4 h, (d) as-prepared powder plus pelletization and sintering at 1250 °C for 4 h, and (e) as-prepared powder plus calcination at 1350 °C for 12 h (showing trace amounts of decomposition products $Nd_4Ga_2O_9$ and Nd_2O_3).

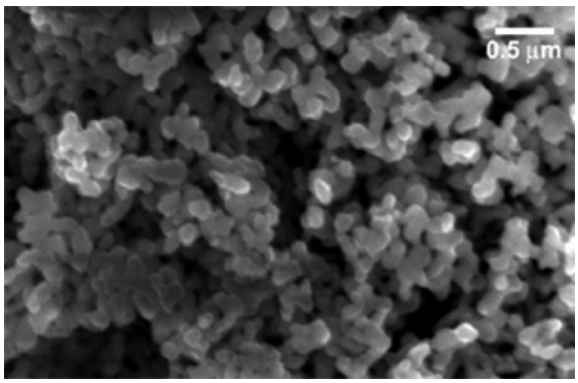

Figure 5. SEM micrograph of a $Nd_3O_2GaO_4$ sample prepared by the combustion technique (see text) and further calcined at 900 °C for 4 h.

combustion synthesis of $Nd_3O_2GaO_4$ (Figure 4a). Similar XRD patterns were observed for all $Nd_4O_4GeO_4$- and $Nd_3O_2GaO_4$-based materials. The as-prepared powders were calcined at different temperatures to determine the minimum temperature required for phase formation. The XRD pattern of the powder calcined at 800 °C for 4 h (Figure 4b) reveals the presence of a small amount of impurity phases of $Nd_4Ga_2O_9$ and Nd_2O_3. However, the pure $Nd_3O_2GaO_4$ phase was obtained when the powder was calcined at 900 °C for 4 h as indicated by the XRD pattern given in Figure 4c. The XRD data suggest that, despite the formation of a small amount of impurities, as in the case of solid-state synthesis, phase pure material can be obtained at temperatures as low as 900 °C probably due to the high reactivity of the combustion-synthesized $Nd_4Ga_2O_9$ and Nd_2O_3. XRD patterns of Zn^{2+} and Mg^{2+} substituted $Nd_3O_2GaO_4$ have also reflected the same kind of behavior. The $Nd_4O_4GeO_4$- and $Nd_3O_2GaO_4$-based materials obtained at 900 °C were used for sintering. Scanning electron microscopy (SEM) micrographs of $Nd_3O_2GaO_4$ powder obtained at 900 °C shows it to consist of spherical particles of about 100−200 nm (Figure 5). The agglomerates seem to be soft in nature and having low strength. High surface energy associated with ultrafine particles is responsible for agglomeration through weak van der Waals forces. No significant partial sintering among particles was observed. The powder seems to be suitable for low-temperature sintering. The SEM observations on all

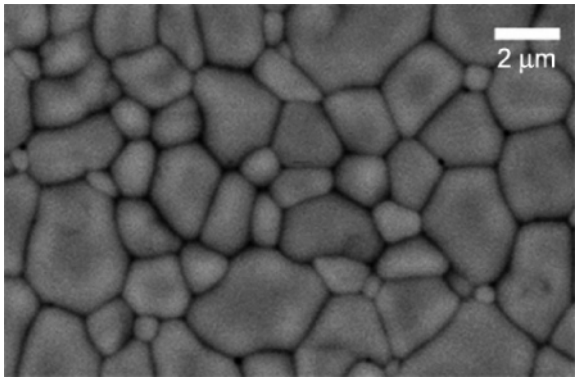

Figure 6. SEM micrograph of a fracture surface of a dense pellet of $Nd_3O_2GaO_4$ sintered at 1250 °C for 4 h.

$Nd_4O_4GeO_4$- and $Nd_3O_2GaO_4$-based materials have also reflected the same kind of morphology of the powders.

The $Nd_4O_4GeO_4$- and $Nd_3O_2GaO_4$-based materials sintered at 1250 °C for 4 h exhibit a density ∼98% of the theoretical. Under such conditions, the pure $Nd_3O_2GaO_4$ phase was obtained as indicated by the XRD pattern given in Figure 4d. The SEM micrograph of $Nd_3Ga_{0.97}Zn_{0.03}O_{5.985}$ sintered 1250 °C for 4 h (Figure 6) reflects the dense microstructure with grain size of about 0.5−4.0 μm. Similar observations were made on $Nd_4O_4GeO_4$-based samples whereas $Nd_3O_2GaO_4$ and Mg^{2+} doped sintered samples exhibited a smaller grain size. The densification of $Nd_4O_4GeO_4$- and $Nd_3O_2GaO_4$-based materials at such a low temperature and without any post-milling step was achieved because of the ultrafine nature of the starting powder associated with high surface area and absence of hard agglomeration among particles. It is important to note that $Nd_3O_2GaO_4$ is not stable above 1300 °C.[2] Figure 4e shows the XRD pattern of the powder calcined at 1350 °C for 12 h, which suggests decomposition of $Nd_3O_2GaO_4$ to form $Nd_4Ga_2O_9$ and Nd_2O_3.

All samples were further analyzed for their cation content by EDX on grains chosen in different areas. For $Nd_3O_2GaO_4$, $Nd_4O_4GeO_4$, and $Nd_4O_{4-x/2}\square_{x/2}(Ge_{1-x}Ga_xO_4)$ materials with $x \geq 0.05$, these elemental analyses gave nominal formulas in very good agreement with the starting compositions. For all other compositions corresponding to smaller substitution rates, the EDX technique is not sensitive enough to analyze the concentration of dopants accurately. However, these dopants were detected and SEM backscattering electron images of samples upon sintering at high temperature were indicative of compositional homogeneity.

3.2. Structural Studies. *(a) $Nd_4O_{4-x/2}\square_{x/2}(Ge_{1-x}Ga_xO_4)$ ($x < 0.125$).* Analysis of XRD patterns recorded for compounds with $x \leq 0.125$ showed that solid solutions are formed up to $x = 0.1$. For $x = 0.125$, diffraction peaks are shifted slightly further with respect to $x = 0.1$ and weak extra peaks corresponding to trace amounts of $Nd_4Ga_2O_9$ and Nd_2O_3 were observed, indicating that the limit of the solid solution is situated between these two latter compositions. Figure 7 illustrates the evolution of the orthorhombic cell parameters with Ga content. As expected, replacement of Ge^{4+} (effective ionic radii in 4-fold coordination: $r_e^{(IV)} = 0.39$ Å)[14] by Ga^{3+}

(14) Shannon, R. D. *Acta Crystallogr., Sect. A* **1976**, *32*, 751.

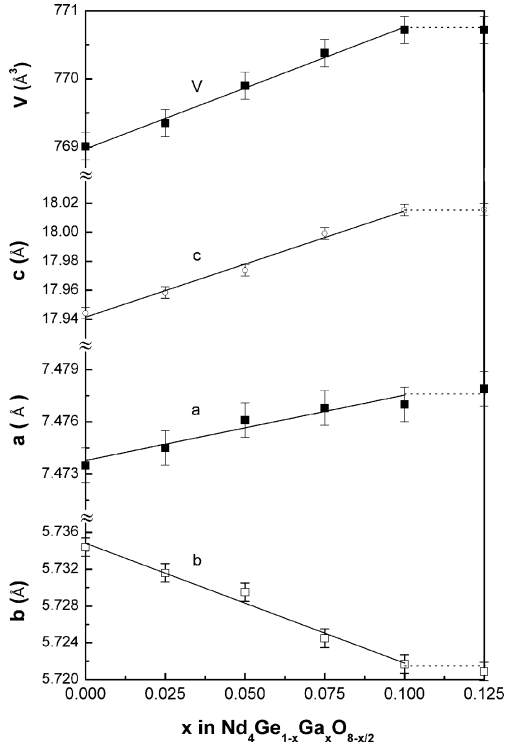

Figure 7. Evolution of cell parameters and cell volume with the Ga content in $Nd_4O_{4-x/2}\square_{x/2}(Ge_{1-x}Ga_xO_4)$ compounds.

Table 1. Cell Parameters of $Nd_3O_2GaO_4$[3] and $Nd_3Ga_{0.97}M_{0.03}O_{5.985}$ (M = Mg and Zn)

	a (Å)	*b* (Å)	*c* (Å)
$Nd_3O_2GaO_4$	9.1820(3)	11.5396(3)	5.5748(3)
$Nd_3Ga_{0.97}Mg_{0.03}O_{5.985}$	9.1842(3)	11.5428(3)	5.5766(3)
$Nd_3Ga_{0.97}Zn_{0.03}O_{5.985}$	9.1894(3)	11.5480(3)	5.5797(3)

($r_e^{(IV)} = 0.47$ Å) induces a volume increase which, though significant, is limited by the compensating effect of oxygen vacancies.

(b) $Nd_3O_{2-x/2}\square_{x/2}(Ga_{1-x}M_xO_4)$ (M = Mg, Zn; x < 0.05). Analysis of XRD data of the sintered samples with $x \leq 0.05$ indicates that solid solutions are formed up to $x = 0.03$ only. For $x = 0.05$, the cell parameters are nearly identical [within three times the estimated standard deviations (esd's)] to those refined for $x = 0.03$ (Table 1), and weak extra peaks corresponding to trace amounts of Nd_2O_3 were observed on the XRD pattern. Extra peaks corresponding to the MO oxide should be observed, but because we are dealing with trace amounts of an oxide of light elements, they can hardly be detected. Such results indicate that the limit of the solid solution is close to $x = 0.03$. Despite its small extent and of the compensating effect of oxygen vacancies, replacement of Ga^{3+} by Mg^{2+} ($r_e^{(IV)} = 0.57$ Å) or Zn^{2+} ($r_e^{(IV)} = 0.60$ Å) does induce a significant volume increase.

(c) $Nd_{3(1-x)}M'_{3x}O_{2-3x/2}\square_{3x/2}(GaO_4)$ (M′ = Ca, Sr; x < 0.05). The XRD data of Ca and Sr substituted samples were analyzed, and the cell parameters were refined. Figure 8 illustrates the evolution of the orthorhombic cell parameters with Ca and Sr content. For M′ = Ca and $x = 0.05$, weak extra peaks corresponding to trace amounts of α-$NdCaGaO_4$,[15,16] CaO and Ga_2O_3 were observed, and the cell parameters are nearly identical (within three times the esd's) to those refined for $x = 0.03$. Similarly, for M′ = Sr and $x = 0.03$, the cell parameters are nearly identical (within three times the esd's) to those refined for $x = 0.015$ and weak extra peaks corresponding to trace amounts of $NdSrGaO_4$,[17] SrO, and Ga_2O_3 were observed. Such results indicate that the limits of the solid solution are close to $x = 0.03$ for Ca and 0.015 for Sr substituted phases.

3.3. Conductivity Measurements. The ac impedance data were analyzed to determine conductivity values of both bulk and grain boundaries and to study electrode phenomena. Data in the form of Nyquist plots are shown in Figure 9 for $Nd_{2.955}Sr_{0.045}GaO_{5.9775}$ (this sample is a good representative of all samples investigated in the course of this study) at different temperatures. In the low temperature range, impedance diagrams mainly show two overlapping semicircles **(**Figure 9a). They have been modeled with the use of an equivalent circuit formed with the series combination of two parallel RC circuits. The least-squares fitting leads to capacitances $C_b \approx 8.7 \pm 0.5$ pF cm^{-1} (the form factor of the sample is 0.27 cm^{-1}) and $C_{gb} \approx 0.9 \pm 0.3$ nF cm^{-1}, which are in good agreement, respectively, with bulk capacitance (high frequency semicircle) and grain boundary capacitance (intermediate frequency semicircle) usually observed in similar materials such as YSZ ($C_b \approx 6.5$ pF cm^{-1} and $C_{gb} \approx 7.3$ nF cm^{-1} in ref 18). As a wide variety of ceramic microstructures occur in practice, it is found that C_{gb} usually lies in the range 10^{-11} to 10^{-8} F cm^{-1}; that rather high values occur in both $Nd_{2.955}Sr_{0.045}GaO_{5.9775}$ and YSZ[18] is indicative of well-sintered samples with narrow intergranular regions.[19] Such capacitance values were used to model part of the electrical behavior at higher temperature (Figure 9b) where strong overlapping of semicircles makes it difficult to distinguish bulk from grain boundary effects. At lower frequency a third semicircle is observed (see inset of Figure 9b). It was modeled with the use of a third parallel RC circuit in series with those representing bulk and grain boundary contributions. The capacitance of this third semicircle, $C_{dl} \approx 7$ μF cm^{-1}, is typical of electrical double layer phenomena, but that the data is in the form of a semicircle rather than a vertical spike is associated with electron transfer to and from the oxide ions at the electrode−ceramic interface; that is, the interface response is partially blocking and has a relatively small R_{dl} resistance. Finally, at the lowest frequencies, a usual inclined spike is observed associated with diffusion-limited processes. It was modeled with a Warburg impedance. In some of the Arrhenius plots given in the next figures, both bulk and total conductivities are displayed in the temperature range where they could be separated accurately.

Although Nd^{3+}, Ga^{3+}, Ge^{4+}, Mg^{2+}, Zn^{2+}, Ca^{2+}, and Sr^{2+} are not known to be prone to either reduction or oxidation,

(15) Daoudi, A.; Demazeau, G.; Le Flem, G. *Rev. Chim. Miner.* **1974**, *11*, 327.
(16) Li, Z.-F.; Li, G.-B.; Liao, F.-H.; Lin, J.-H. *J. Solid State Chem.* **2003**, *172*, 59.
(17) Vasylechko, L. O.; Fedorchuk, A. A.; Savitskii, D. I.; Matkovskii, A. O.; Ubizskii, S. B. *Inorg. Mater.* **1995**, *31* (9), 1128.
(18) Ruiz-Morales, J. C.; Marrero-Lüpez, D.; Irvine, J. T. S.; Núñez, P. *Mater. Res. Bull.* **2004**, *39*, 1299.
(19) Irvine, J. T. S.; Sinclair, D. C.; West, A. R. *Adv. Mater.* **1990**, *2* (3), 132.

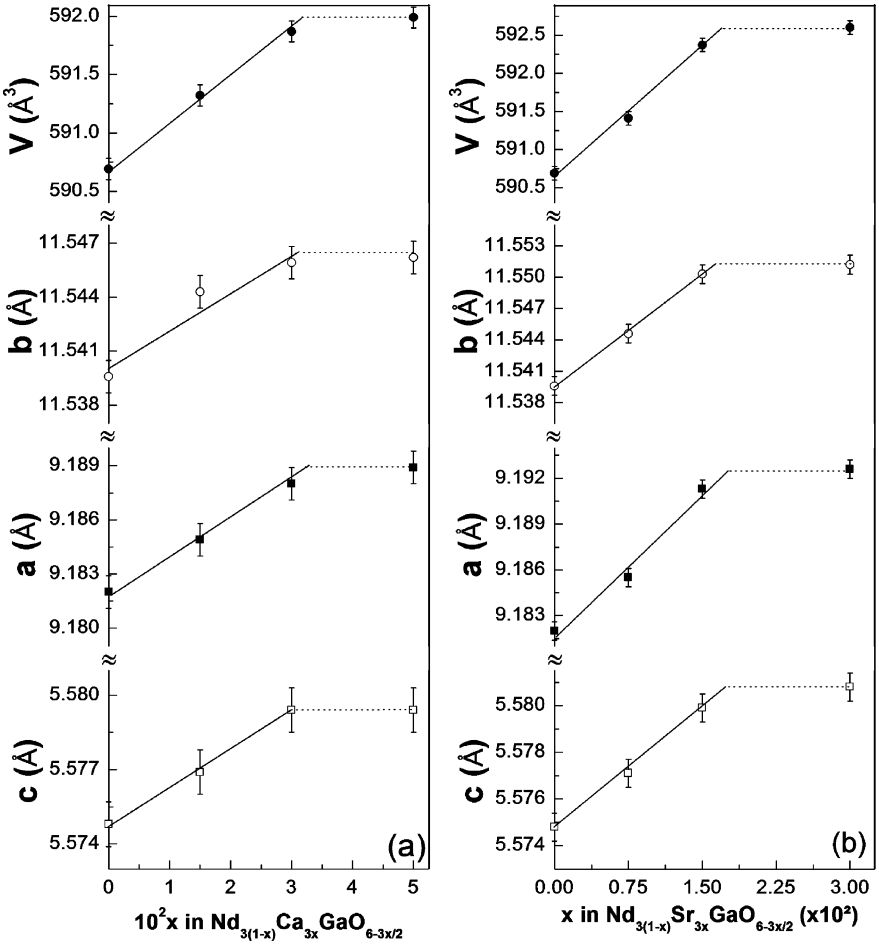

Figure 8. Evolution of cell parameters and cell volume with the M′ content in $Nd_{3(1-x)}M'_{3x}O_{2-3x/2}\square_{3x/2}(GaO_4)$ compounds: (a) M′ = Ca and (b) M′ = Sr.

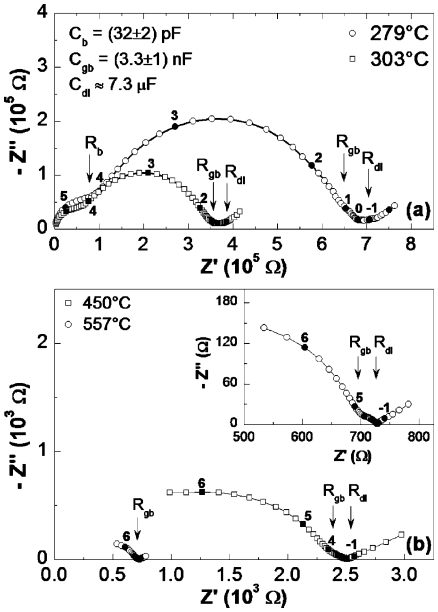

Figure 9. Complex impedance plane plots (figures on the curves denote decades of frequency) for $Nd_{2.955}Sr_{0.045}GaO_{5.9775}$ at various temperatures (the solid lines are the fittings). An enlarged image of the impedance plot at 557 °C is given in the inset of part b.

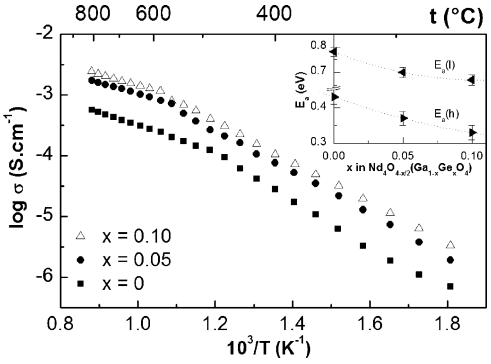

Figure 10. Conductivity data for $Nd_4O_{4-x/2}\square_{x/2}(Ge_{1-x}Ga_xO_4)$ compounds.

all compounds were subjected to conductivity measurements under two reduced oxygen partial pressures (10^{-5} and 10^{-20} atm). As expected, it was shown that, within experimental error, the conductivities are almost identical to those measured in dry air which indicates that the ionic conductivity is clearly dominant in these materials. Consequently, because the mobility of cationic species mentioned above is very likely negligible, one can conclude that the title materials are pure oxide−ion conductors.

(a) $Nd_4O_{4-x/2}\square_{x/2}(Ge_{1-x}Ga_xO_4)$ ($x < 0.125$) Compounds. Conductivity results are given in the form of Arrhenius plots in Figure 10. In all cases, the evolution of the conductivity with temperature exhibits two thermally activated regimes with a break at a temperature ranging from ∼450 °C for $x = 0$ to ∼550 °C for $x = 0.1$. This feature could be related to a ferroelectric−paraelectric phase transition, that is, a structural change from SG $Pmc2_1$ to SG *Pmcm* (or *Pmcn*).[1] This possible transition is being investigated by dielectric (temperature dependence of the permittivity) and microcalorimetric measurements. In the low-temperature regime,

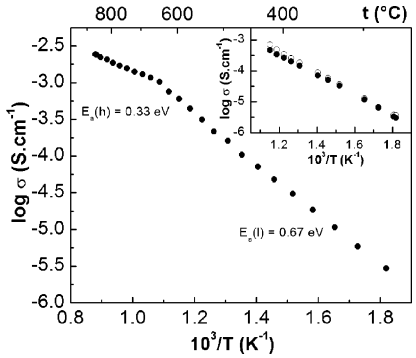

Figure 11. Arrhenius plots for $Nd_4Ge_{0.9}Ga_{0.1}O_{7.95}$ (bulk and total conductivities are represented by open and filled circles, respectively).

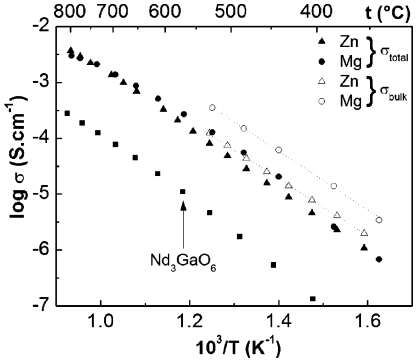

Figure 12. Conductivity data for $Nd_3O_2GaO_4$ and $Nd_3Ga_{0.97}M_{0.03}O_{5.985}$ (M = Zn and Mg; total and bulk conductivities are represented by filled and open markers, respectively; squares for $Nd_3O_2GaO_4$, triangles for M = Mg, and circles for M = Zn).

the activation energy E_a(l) is larger than that at higher temperature E_a(h) (Figure 10). Both E_a(l) and E_a(h) values decrease when x increases as a probable consequence of a weaker covalent framework. As expected, when Ga^{3+} is substituted for Ge^{4+}, charge-compensating oxygen vacancies play a beneficial role on the anionic conductivity which increases from 2.8×10^{-4} S cm^{-1} for pure Nd_4GeO_8 to 1.9×10^{-3} S cm^{-1} for $x = 0.1$, at 800 °C. For this latter composition, the evolution of both bulk and total conductivities is displayed in Figure 11.

(b) $Nd_3O_{2-x/2}\square_{x/2}(Ga_{1-x}M_xO_4)$ (M = Mg, Zn; x < 0.05). Figure 12 shows the ion conductivity of $Nd_3O_2GaO_4$ and $Nd_3O_{1.985}\square_{0.015}(Ga_{0.97}M_{0.03}O_4)$ (M = Zn, Mg) compounds, as a function of temperature. All curves reflect the expected Arrhenius kind of behavior. The conductivity for pure $Nd_3O_2GaO_4$ at 800 °C was found to be 2.7×10^{-4} S cm^{-1} with an activation energy of 1.2 eV.

Despite limited substitution rates of Zn^{2+} and Mg^{2+} for Ga^{3+} in $Nd_3O_2GaO_4$ (as demonstrated by XRD analysis) a significant improvement in the ionic conductivity was observed. The ionic conductivity for $Nd_3O_2GaO_4$ doped with 3% Zn^{2+} and Mg^{2+} was found to be 0.5×10^{-2} and 0.4×10^{-2} S cm^{-1} at 800 °C, with activation energies of 1.08 and 1.2 eV, respectively.

The difference between bulk and total conductivities in the case of the Mg-substituted compound is larger than for the Zn-doped material (Figure 12), although both samples had almost the same density. This result is likely related to the smaller grain size of the Mg- compared to the Zn-doped sample, thus, leading to a larger grain boundary effect.

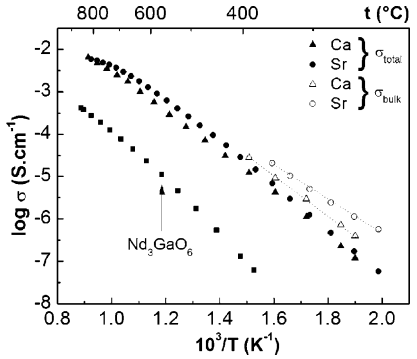

Figure 13. Conductivity data for $Nd_3O_2GaO_4$, $Nd_{2.91}Ca_{0.09}GaO_{5.955}$, and $Nd_{2.955}Sr_{0.045}GaO_{5.9775}$ (total and bulk conductivities are represented by filled and open markers, respectively; squares for $Nd_3O_2GaO_4$, triangles for $Nd_{2.91}Ca_{0.09}GaO_{5.955}$, and circles for $Nd_{2.955}Sr_{0.045}GaO_{5.9775}$).

(c) $Nd_{3(1-x)}M'_{3x}O_{2-3x/2}\square_{3x/2}(GaO_4)$ (M′ = Ca, Sr; x < 0.05). The oxygen ion conductivity of $Nd_3O_2GaO_4$, $Nd_{2.91}Ca_{0.09}GaO_{5.955}$, and $Nd_{2.955}Sr_{0.045}GaO_{5.9775}$ compounds, as a function of temperature, is shown in Figure 13. As in the case of Zn^{2+} and Mg^{2+} substituted compounds, it can be seen that the creation of a small rate of oxygen vacancies in the $Nd_3O_2GaO_4$ structure, concomitant with substitutions of Ca^{2+} and Sr^{2+} for Nd^{3+}, induces a significant increase of the anionic conductivity which reaches 0.6×10^{-2} and 0.7×10^{-2} S cm^{-1}, at 800 °C, for $Nd_{2.91}Ca_{0.09}GaO_{5.955}$ and $Nd_{2.955}Sr_{0.045}GaO_{5.9775}$, respectively. Activation energies for these Ca and Sr substituted compounds, 0.97 and 1.06 eV, respectively, are, as expected, rather close to those of other $Nd_3O_2GaO_4$-based materials.

4. Conclusion

A novel wet-chemical process based on EDTA−nitrate combustion has been developed, which has a potential to produce phase-pure, ultrafine, well-sinterable powders of $Nd_4O_4GeO_4$- and $Nd_3O_2GaO_4$-based materials. They have been characterized by XRD on powder samples. It was found that cation substitution with lower valent cations to form charge-compensating oxygen vacancies was possible only at the Ge^{4+} site of $Nd_4O_4GeO_4$ and at both cation sites of $Nd_3O_2GaO_4$. However, it was observed that both structures are not very prone to accept large rates of oxygen vacancies. $Nd_4Ge_{1-x}Ga_xO_{8-x/2}$ is formed up to $x = 0.10$, $Nd_3Ga_{1-x}M_xO_{6-x/2}$ (M = Zn, Mg) up to $x = 0.03$, and $Nd_{3(1-x)}M'_{3x}GaO_{6-3x/2}$ up to $x = 0.03$ and 0.015 for M′ = Ca and Sr, respectively. Despite these small substitution rates, significant improvements of the anionic conductivity are observed for all substituted compounds.

Acknowledgment. R.D.P. gratefully acknowledges financial support of the "Région des Pays de la Loire" in the form of a postdoctoral fellowship for 11 months. A.L. gratefully acknowledges financial support of the University of Nantes in the form of an invited professorship for 5 months. Partial support of Wake Forest University through a R. J. Reynolds research sabbatical leave award is acknowledged.

CM050537H